PROCEEDINGS OF SCIENCE

Angular analysis and branching ratio of the $B^0 \to K^{*0}\mu^+\mu^-$ decay

Mauro Dinardo[*†]
INFN and Unversity of Milano Bicocca
E-mail: mauro.dinardo@cern.ch

The angular distributions and the differential branching fraction of the $B^0 \to K^{*0}\mu^+\mu^-$ decay are studied using an integrated luminosity of $5.2\,fb^{-1}$ of data, collected with the CMS detector. The forward-backward asymmetry of the muons A_{FB}, the K^{*0} longitudinal polarization fraction F_L, and the differential branching fraction $d\mathscr{B}/dq^2$, are determined as a function of the dimuon invariant mass squared. The measurements are in good agreement with the standard model.

14th International Conference on B-Physics at Hadron Machines
April 8-12, 2013
Bologna, Italy

[*]Speaker.
[†]On behalf of the CMS collaboration.

PoS(Beauty 2013)029

1. Introduction

One productive area where searching for new phenomena beyond the standard model (SM), is the study of flavor-changing neutral current decays of b hadrons, such as the decay mode $\mathrm{B}^0 \to \mathrm{K}^{*0}\mu^+\mu^-$. This decay is forbidden at tree level in the SM, resulting in small expected rates. From a theoretical side, robust calculations are now available, and they indicate that new physics could give rise to sizable effects. Finally, this decay mode is relatively easy to select and reconstruct at hadron colliders. Two important observables in the $\mathrm{B}^0 \to \mathrm{K}^{*0}\mu^+\mu^-$ decay are the forward-backward asymmetry of the muons, A_{FB}, and the longitudinal polarization fraction of the $\mathrm{K}^*(892)$, F_L. These can be measured as a function of the q^2 of the decay (dimuon invariant mass squared) and then compared to SM predictions [12, 6, 9].

While previous measurements by BaBar, Belle, CDF, and LHCb are consistent with the SM [4, 15, 3, 1], these are still statistically limited and new results may provide an indication of new physics. This paper presents measurements of A_{FB}, F_L, and the differential branching fraction $\mathrm{d}\mathscr{B}/\mathrm{d}q^2$ from $\mathrm{B}^0 \to \mathrm{K}^{*0}\mu^+\mu^-$ decays, using data collected from pp collisions at the Compact Muon Solenoid (CMS) experiment in 2011, at a center of mass energy of 7 TeV. Analyzed data corresponds to an integrated luminosity of $5.2 \pm 0.1\,\mathrm{fb}^{-1}$. A detailed description of the CMS detector can be found in Ref. [10], while details on the analysis, in particular on the event selection, are available in Ref. [11].

2. Analysis

Figure 1 shows the relevant angular observables needed to define the decay: θ_K is the angle between the kaon momentum and the direction opposite to the B^0 $\left(\overline{\mathrm{B}}^0\right)$ in the K^{*0} $\left(\overline{\mathrm{K}}^{*0}\right)$ rest frame, θ_l is the angle between the positive (negative) muon momentum and the direction opposite to the B^0 $\left(\overline{\mathrm{B}}^0\right)$ in the dimuon reference frame, and ϕ is the angle between the plane containing the two muons and the plane containing the kaon and the pion. As the extracted angular parameters A_{FB} and F_L do not depend on ϕ and the acceptance times efficiency is flat as a function of ϕ, the ϕ variable is integrated out. Although the $\mathrm{K}^+\pi^-$ invariant mass must be consistent with a K^{*0}, there can be contributions from a spinless (S-wave) $\mathrm{K}^+\pi^-$ combination which can be parameterized with two terms related to the S-wave fraction, F_S, and to the interference between the S-wave and P-wave decays, A_S. Including this component, the angular distribution of the $\mathrm{B}^0 \to \mathrm{K}^{*0}\mu^+\mu^-$ can be written as [5]:

$$\begin{aligned}\frac{1}{\Gamma}\frac{\mathrm{d}^3\Gamma}{\mathrm{d}\cos\theta_K\,\mathrm{d}\cos\theta_l\,\mathrm{d}q^2} = \frac{9}{16}\Bigg\{ & \left[\frac{2}{3}F_S + \frac{4}{3}A_S\cos\theta_K\right]\left(1-\cos^2\theta_l\right) + \\ & + \left(1-F_S\right)\Big[2F_L\cos^2\theta_K\left(1-\cos^2\theta_l\right) + \\ & + \frac{1}{2}\left(1-F_L\right)\left(1-\cos^2\theta_K\right)\left(1+\cos^2\theta_l\right) + \\ & + \frac{4}{3}A_{FB}\left(1-\cos^2\theta_K\right)\cos\theta_l\Big]\Bigg\}. \end{aligned} \tag{2.1}$$

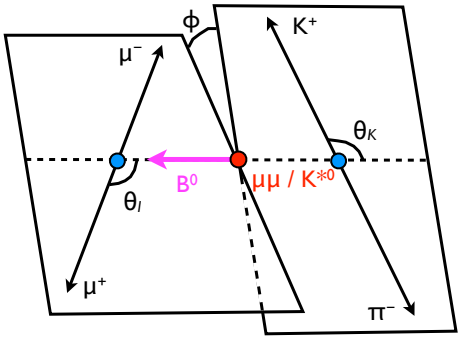

Figure 1: Sketch showing the definition of the angular observables for the decay $\mathrm{B}^0 \to \mathrm{K}^{*0}\mu^+\mu^-$.

The main results of the analysis are extracted from unbinned extended maximum likelihood fits to three variables: the B^0 invariant mass and the two angular variables θ_K and θ_l. For each q^2 bin, the probability density function has the following mathematical expression:

$$\begin{aligned} \text{p.d.f.}(m,\cos\theta_K,\cos\theta_l) = {} & Y_S\, S(m)\cdot S(\cos\theta_K,\cos\theta_l)\cdot\varepsilon(\cos\theta_K,\cos\theta_l) + \\ & + Y_B^c\, B^c(m)\cdot B^c(\cos\theta_K)\cdot B^c(\cos\theta_l) + \\ & + Y_B^p\, B^p(m)\cdot B^p(\cos\theta_K)\cdot B^p(\cos\theta_l). \end{aligned} \tag{2.2}$$

The signal yield is given by the free parameter Y_S and the signal shape is described by the function $S(m)$, in the invariant mass variable, and by the product of the theoretical signal shape in the two angular variables, $S(\cos\theta_K,\cos\theta_l)$, and the efficiency in the two angular variables, $\varepsilon(\cos\theta_K,\cos\theta_l)$. The signal mass shape $S(m)$ is a sum of two Gaussians with a common mean. While the mean is free to float, the two resolution parameters and the relative fraction are fixed to the result of a fit to simulated events. The signal angular function $S(\cos\theta_K,\cos\theta_l)$ is given by Eq. 2.1. The efficiency function $\varepsilon(\cos\theta_K,\cos\theta_l)$ is a polynomial in $\cos\theta_l$ and $\cos\theta_K$ and is obtained by fitting two-dimensional efficiency histograms. There are two contributions to the background, with yields given by Y_B^p for the "peaking" background and Y_B^c for the "combinatorial" background. The peaking background is due to feed-through from $\mathrm{B}^0 \to \mathrm{K}^{*0}J/\psi$ and $\mathrm{B}^0 \to \mathrm{K}^{*0}\psi'$ decays. The shapes of this background in the mass, $B^p(m)$, and angular variables, $B^p(\cos\theta_K)$ and $B^p(\cos\theta_l)$, are obtained from simulation. The remaining background, combinatorial in nature, is described by a single exponential in mass, $B^c(m)$, and a polynomial, as needed to describe the data, in each angular variable, $B^c(\cos\theta_K)$ and $B^c(\cos\theta_l)$. In the fits to the data, the parameters that define the shapes of $S(m)$, $B^p(m)$, $B^p(\cos\theta_K)$, and $B^p(\cos\theta_l)$ (except the mass parameter in $S(m)$), as well as the yield Y_B^p, are initially set to the values obtained from simulation, with a Gaussian constraint defined by the uncertainty found in the fit to the simulated events. The fit has been carried out to the $\mathrm{B}^0 \to \mathrm{K}^{*0}J/\psi$ channel first and the values for F_S and A_S are extracted and used in the signal q^2 bins, with Gaussian constraints defined by the uncertainty from the fit.

The differential branching fraction, $\mathrm{d}\mathscr{B}/\mathrm{d}q^2$, is measured relative to the normalization channel

Table 1: Systematic uncertainty contributions for the measurements of F_L, A_{FB}, and $\mathrm{d}\mathscr{B}/\mathrm{d}q^2$.

Systematic uncertainty	F_L	A_{FB}	$\mathrm{d}\mathscr{B}/\mathrm{d}q^2$
Efficiency statistical uncertainty	0.005 – 0.007	0.003 – 0.005	1%
Potential bias from fit algorithm (toy MC)	0.003 – 0.040	0.012 – 0.077	0 – 2.7%
Potential bias from fit ingredients (full MC)	0	0 – 0.017	0 – 7.1%
Incorrect CP assignment of decay	0.002 – 0.006	0.002 – 0.006	0
Effect of Kπ S-wave contribution	0.005 – 0.023	0.006 – 0.014	5%
Peaking background mass shape	0 – 0.026	0 – 0.008	0 – 15.2%
Combinatorial background shapes vs $\cos\theta_{L,K}$	0.003 – 0.179	0.004 – 0.161	0 – 3.3%
Angular resolution	0 – 0.019	0	0
Signal mass shape	0	0	0.9%
Efficiency shape	0.016	0.004	14.3%
Total systematic uncertainty	0.031 – 0.186	0.018 – 0.179	(15.5 – 21.5)%

$\mathrm{B}^0 \to \mathrm{K}^{*0} J/\psi$ and multiplied by the known branching fraction for this channel:

$$\frac{\mathrm{d}\mathscr{B}\left(\mathrm{B}^0 \to \mathrm{K}^{*0}\mu^+\mu^-\right)}{\mathrm{d}q^2} = \frac{Y_S}{Y_N}\frac{\varepsilon_N}{\varepsilon_S}\frac{\mathscr{B}\left(\mathrm{B}^0 \to \mathrm{K}^{*0} J/\psi\right)}{\mathrm{d}q^2}, \tag{2.3}$$

where Y_S, Y_N are the yields of the signal and normalization channels, respectively, ε_S, ε_N are the efficiencies of the signal and normalization channels, respectively, and $\mathscr{B}\left(\mathrm{B}^0 \to \mathrm{K}^{*0} J/\psi\right)$ is the world average branching fraction for the normalization channel [14]. The yields are obtained by fits to the invariant mass distributions and the efficiencies are obtained by integrating over the angular variables, using the values obtained from the fits described previously. A summary of the systematic uncertainties is given in Table 1, where the ranges give the variation over the q^2 bins.

3. Results

The $\mathrm{B}^0 \to \mathrm{K}^{*0} J/\psi$ decay is used to validate the fit and obtain the values for F_S and A_S used in the fits to the signal q^2 bins. From 47 000 $\mathrm{B}^0 \to \mathrm{K}^{*0} J/\psi$ events, the longitudinal polarization fraction is measured to be $F_L = 0.554 \pm 0.004(\mathrm{stat.})$, the dimuon forward-backward asymmetry is found to be $A_{FB} = -0.004 \pm 0.004(\mathrm{stat.})$, the scalar fraction is $F_S = 0.01 \pm 0.01(\mathrm{stat.})$, and the scalar-vector interference term is determined to be $A_S = -0.10 \pm 0.01(\mathrm{stat.})$. The result for F_L is consistent with the world average value of 0.570 ± 0.008, while the value for A_{FB} is compatible with the expected result of no asymmetry.

The $\mathrm{K}^+\pi^-\mu^+\mu^-$ invariant mass distributions for each q^2 bin of the signal sample $\mathrm{B}^0 \to \mathrm{K}^{*0}\mu^+\mu^-$ are shown in Fig. 2, along with the projection of the unbinned maximum likelihood fit described in Sec. 2. From the fit, the K^{*0} longitudinal polarization fraction F_L and the forward-backward asymmetry of the muons A_{FB} are obtained in bins of q^2. These results are shown in Fig. 3, along with SM predictions [8]. The branching fraction for $\mathrm{B}^0 \to \mathrm{K}^{*0}\mu^+\mu^-$ is obtained as a function of q^2 and shown in Fig. 4, together with the SM predictions.

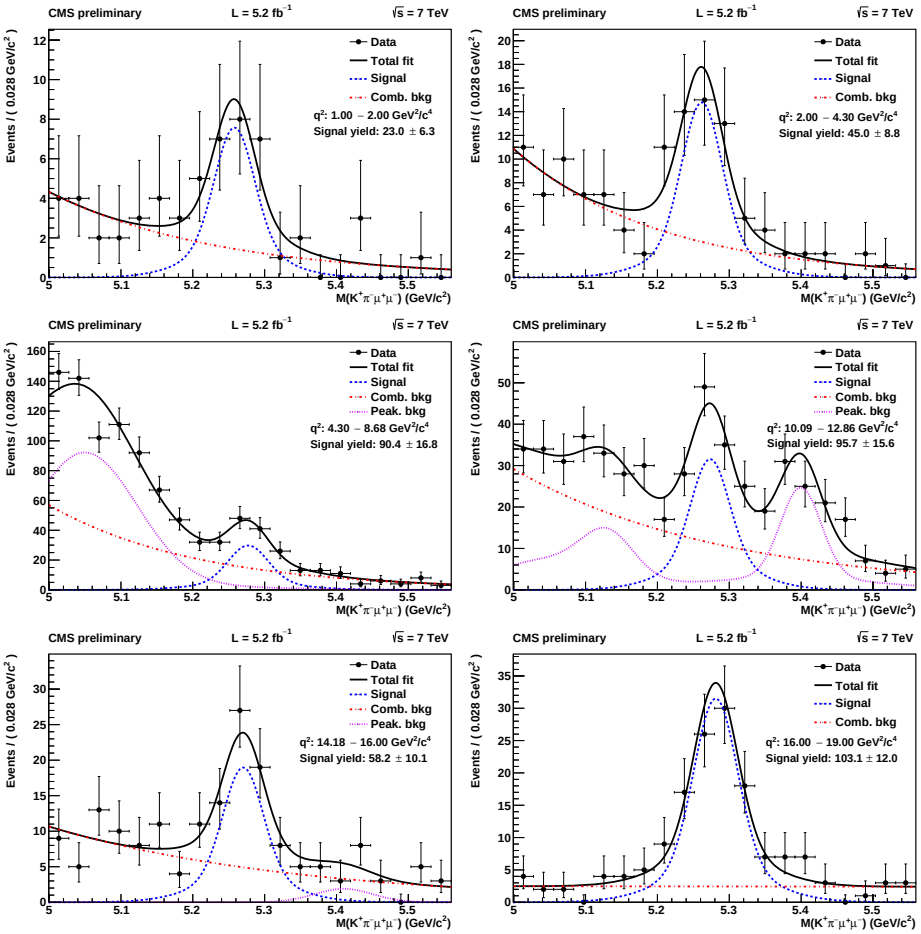

Figure 2: The $K^+\pi^-\mu^+\mu^-$ invariant mass distributions for each of the signal q^2 bins. Overlaid on each mass distribution is the projection of the unbinned maximum likelihood fit described in Sec. 2.

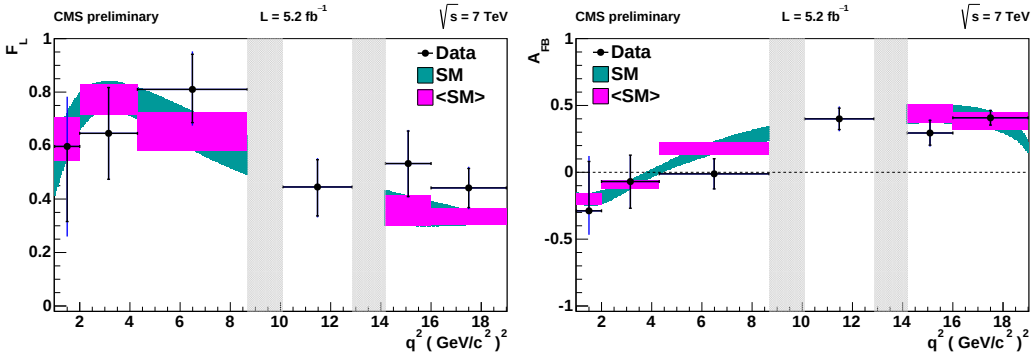

Figure 3: Results of the measurement of F_L (left) and A_{FB} (right) versus the dimuon q^2. The statistical uncertainty on the data points is shown by shorter error bars while the longer error bars give the total uncertainty. The gray shaded regions correspond to the J/ψ and ψ' resonances. The SM prediction is given by the cyan (light) band. The magenta (dark) regions represent the SM prediction averaged within the q^2 bins to allow direct comparison to the data points.

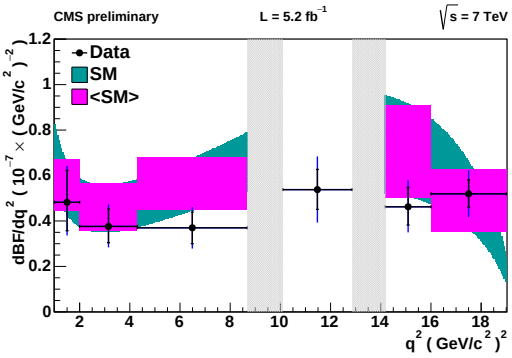

Figure 4: Results of the measurement of $\mathrm{d}\mathscr{B}/\mathrm{d}q^2$ versus the dimuon q^2. The statistical uncertainty on the data points is shown by shorter error bars while the longer error bars give the total uncertainty (not including the 4.6% normalization uncertainty). The gray shaded regions correspond to the J/ψ and ψ' resonances. The SM prediction is given by the cyan (light) band. The magenta (dark) regions represent the SM prediction averaged within the q^2 bins to allow direct comparison to the data points.

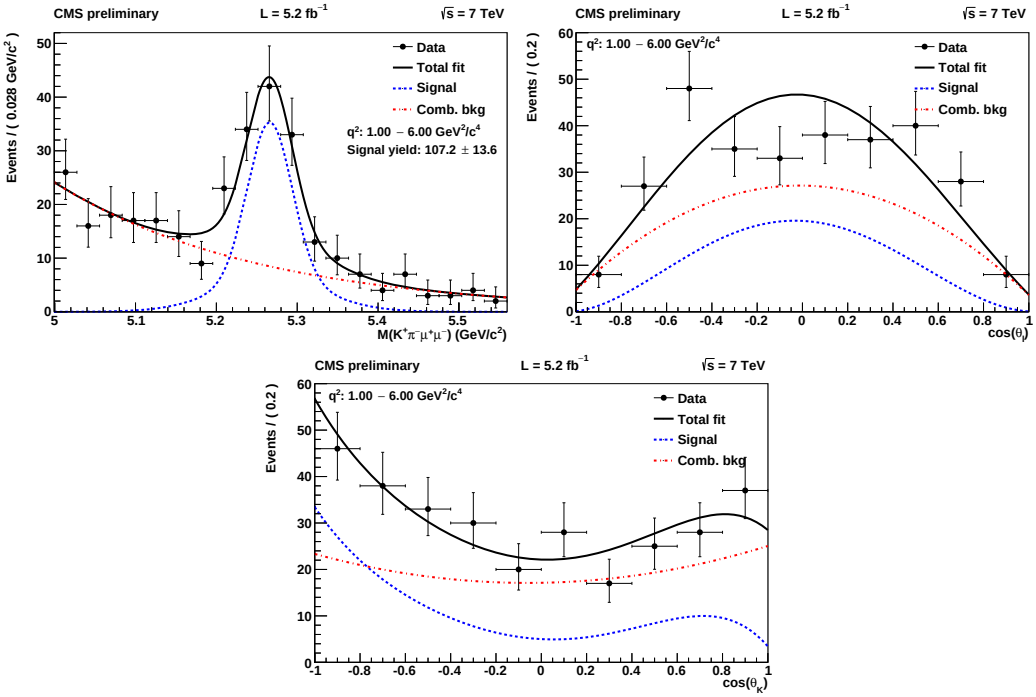

Figure 5: The $\mathrm{K}^+\pi^-\mu^+\mu^-$ invariant mass (top left), $\cos\theta_l$ (top right), and $\cos\theta_K$ (bottom) distributions for $1 < q^2 < 6$ $(\mathrm{GeV}/c^2)^2$, along with projections of the unbinned maximum likelihood fit.

The angular observables can be theoretically predicted with good control of the relevant form factor uncertainties in the low dimuon invariant mass region. It is therefore interesting to perform the measurements of the relevant observables in the $1 < q^2 < 6\,(\mathrm{GeV}/c^2)^2$ region. The results in this region, along with the fit projections, are shown in Fig. 5. The values obtained from this fit are: $F_L = 0.68 \pm 0.10(\mathrm{stat.}) \pm 0.02(\mathrm{syst.})$, $A_{FB} = -0.07 \pm 0.12(\mathrm{stat.}) \pm 0.01(\mathrm{syst.})$, and $\mathrm{d}\mathscr{B}/\mathrm{d}q^2 = (4.4 \pm 0.6(\mathrm{stat.}) \pm 0.7(\mathrm{syst.})) \times 10^{-8}\,c^4/\mathrm{GeV}^2$, where the systematic uncertainty on $\mathrm{d}\mathscr{B}/\mathrm{d}q^2$ does not include the 4.6% normalization uncertainty. These results are consistent with the SM predictions of $F_L = 0.74^{+0.06}_{-0.07}$, $A_{FB} = -0.04 \pm 0.03$, and $\mathrm{d}\mathscr{B}/\mathrm{d}q^2 = (4.9^{+1.0}_{-1.1}) \times 10^{-8}\,c^4/\mathrm{GeV}^2$ [7].

The CMS measurements versus q^2 of A_{FB}, F_L, and the branching fraction are compared to previously published measurements that use the same q^2 binning [15, 3, 2, 13, 1] in Fig. 6. The CMS measurements are more precise than all but the LHCb values, and in the highest q^2 bin the CMS measurements have the smallest uncertainty on A_{FB} and F_L.

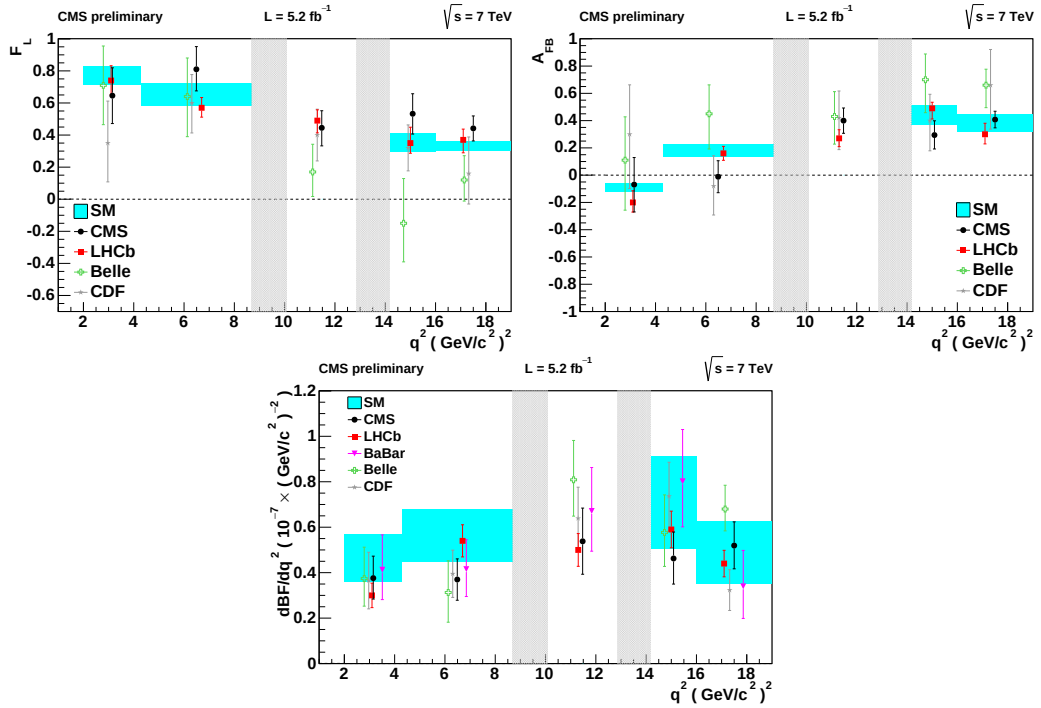

Figure 6: Measurements versus q^2 of F_L (top left), A_{FB} (top right), and branching fraction (bottom) for $\mathrm{B} \to \mathrm{K}^* \ell^+ \ell^-$ from CMS (this paper), Belle [15], CDF [3, 2], BaBar [13], and LHCb [1]. The error bars give the total uncertainty. The gray shaded regions correspond to the J/ψ and ψ' resonances. The cyan regions represent the SM prediction averaged within the q^2 bins to allow direct comparison to the data points.

References

[1] R. Aaij et al. Differential branching fraction and angular analysis of the decay $\mathrm{B}^0 \to \mathrm{K}^{*0}\mu^+\mu^-$. 2013.

[2] T. Aaltonen et al. Measurement of the forward-backward asymmetry in the $\mathrm{B} \to \mathrm{K}^{(*)}\mu^+\mu^-$ decay and first observation of the $\mathrm{B}_s \to \phi\mu^+\mu^-$ decay. *Phys. Rev. Lett.*, 106:161801, 2011.

[3] T. Aaltonen et al. Measurements of the angular distributions in the decays $B \to K^{(*)}\mu^+\mu^-$ at CDF. *Phys. Rev. Lett.*, 108:081807, 2012.

[4] Bernard Aubert et al. Angular distributions in the decay $B \to K^*\ell^+\ell^-$. *Phys. Rev. D*, 79:031102, 2009.

[5] Thomas Blake, Ulrik Egede, and Alex Shires. The effect of S-wave interference on the $B^0 \to K^{*0}\ell^+\ell^-$ angular observables. *JHEP*, 03:027, 2013.

[6] Christoph Bobeth, Gudrun Hiller, and Danny van Dyk. The benefits of $\overline{B} \to \overline{K}^*\ell^+\ell^-$ decays at low recoil. *JHEP*, 1007:098, 2010.

[7] Christoph Bobeth, Gudrun Hiller, and Danny van Dyk. More benefits of semileptonic rare B decays at low recoil: CP violation. *JHEP*, 1107:067, 2011.

[8] Christoph Bobeth, Gudrun Hiller, and Danny van Dyk. General analysis of $\overline{B} \to \overline{K}^{(*)}\ell^+\ell^-$ decays at low recoil. *Phys. Rev. D*, 87:034016, 2012.

[9] Christoph Bobeth, Gudrun Hiller, Danny van Dyk, and Christian Wacker. The decay $\overline{B} \to \overline{K}\,\ell^+\ell^-$ at low hadronic recoil and model-independent $\Delta B = 1$ constraints. *JHEP*, 1201:107, 2012.

[10] S. Chatrchyan et al. The CMS experiment at the CERN LHC. *JINST*, 3:S08004, 2008.

[11] CMS Collaboration. Angular analysis and branching ratio measurement of the decay $B \to K^{*0}\mu^+\mu^-$. CMS PAS BPH-11-009, 2013.

[12] Frank Krüger, Lalit M. Sehgal, Nita Sinha, and Rahul Sinha. Angular distribution and cp asymmetries in the decays $\overline{B} \to K^-\pi^+e^-e^+$ and $\overline{B} \to \pi^-\pi^+e^-e^+$. *Phys. Rev. D*, 61:114028, 2000.

[13] J.P. Lees et al. Measurement of branching fractions and rate asymmetries in the rare decays $B \to K^{(*)}\ell^+\ell^-$. *Phys. Rev. D*, 86:032012, 2012.

[14] Particle Data Group, J. Beringer, et al. Review of Particle Physics. *Phys. Rev. D*, 86:010001, 2012.

[15] J.-T. Wei et al. Measurement of the differential branching fraction and forward-backword asymmetry for $B \to K^{(*)}\ell^+\ell^-$. *Phys. Rev. Lett.*, 103:171801, 2009.